

Nonlinear Annihilation of Excitations in Photosynthetic Systems

Leonas Valkunas,* Gediminas Trinkunas,* Vldas Liuolia,* and Rienk van Grondelle[‡]

*Institute of Physics, Vilnius 2600, Lithuania, and [‡]Free University of Amsterdam, 1081 HV Amsterdam, The Netherlands

ABSTRACT The theory of the singlet-singlet annihilation in quasi-homogeneous photosynthetic antenna systems is developed further. In the new model, the following important contributions are taken into account: 1) the finite excitation pulse duration, 2) the occupation of higher excited states during the annihilation, 3) excitation correlation effects, and 4) the effect of local heating. The main emphasis is concentrated on the analysis of pump-probe kinetic measurements demonstrating the first two above possible contributions. The difference with the results obtained from low-intensity fluorescence kinetic measurements is highlighted. The experimental data with picosecond time resolution obtained for the photosynthetic bacterium *Rhodospirillum rubrum* at room temperature are discussed on the basis of this theory.

INTRODUCTION

The light-harvesting antenna (LHA) of photosynthetic systems is the major absorber of solar energy. In the LHA, excitation energy is transferred very efficiently to reaction centers (RC), where the electronic excitation energy is converted into a stable charge separation. The determination of the molecular and structural parameters of the LHA that govern the energy migration process is a crucial problem. To obtain these parameters, two different types of experimental approaches have been used. In the first type of experiment, the low-intensity excitation decay kinetics are measured (see, e.g., Godik et al., 1988; Van Grondelle et al., 1987; Freiberg et al., 1989; Holzwarth, 1991; Werst et al., 1992; Timpmann et al., 1991), and the excitation migration parameters can be extracted directly if the excitation decay process is (close to) migration-limited. If this is not the case, the excitation decay kinetics is strongly influenced by the excitation trapping rate at the RC and, consequently, no information about the excitation migration is obtained from such experiments. The second experimental strategy to study the excitation transfer in the LHA is to measure the decay of the excitation density due to nonlinear annihilation. In this case, the excitation kinetics is determined by their mutual interaction and, therefore, this process is migration-limited, at least under medium excitation intensities. From the analysis of singlet-singlet (Paillotin et al., 1979; Den Hollander et al., 1983; Bakker et al., 1983; Van Grondelle, 1985; Kudzmauskas et al., 1988; Valkunas, 1989; Trinkunas and Valkunas, 1989) or singlet-triplet (Monger and Parson, 1977; Breton et al., 1983; Paillotin et al., 1983) annihilation, the energy migration parameters in the LHA can be obtained. At room temperature, the excitation decay due to trapping in the RC takes less than 100 ps. For simple photosynthetic systems with only a single long-wavelength

antenna absorption band, such as *Rhodospirillum (Rs.) rubrum*, the observed low-excitation intensity kinetics is close to exponential (Godik et al., 1988; Van Grondelle et al., 1987; Freiberg et al., 1989; Timpmann et al., 1991). In photosynthetic systems with a more complicated LHA containing several spectral forms, a multi-exponential decay is measured. Also, in this case the slowest exponent, representing the trapping process, is <100 ps (Freiberg et al., 1989; Van Grondelle and Sundström, 1991; Visscher et al., 1989). On the other hand, measurements at low temperatures of the low-intensity excitation decay kinetics in the LHA of the photosynthetic purple bacterium *Rs. rubrum* clearly exhibit multi-exponential behavior (Timpmann et al., 1991) related to what is observed for complicated LHAs. Moreover, at low temperatures the observed kinetics depends strongly on the selected excitation/recording wavelengths. These results have led to the conclusion that even the simplest long-wavelength LHA is spectrally inhomogeneous (Godik et al., 1988; Freiberg et al., 1989; Timpmann et al., 1991). The wavelength dependence of the fluorescence quantum yield on the intensity of the exciting laser pulse at low temperatures further shows the presence of different spectral forms in the long-wavelength bacterial LHA (Deinum et al., 1989; Deinum, 1991), whereas at room temperature the spectral inhomogeneity is no longer apparent. The current theoretical description of the nonlinear excitation decay kinetics is based mainly upon energy transfer and trapping on a homogeneous molecular lattice (Paillotin et al., 1979; Den Hollander et al., 1983; Kudzmauskas et al., 1988; Valkunas, 1989; Trinkunas and Valkunas, 1989; Suna, 1970; Gaididei et al., 1985) and, therefore, can be directly applied to the analysis of the room temperature results. In small LHA domains (small in comparison with the excitation diffusion radius), annihilation is very efficient. As a consequence, the behavior of the fluorescence quantum yield upon increasing the excitation intensity is determined largely by fluctuations in the number of excitations per domain at a fixed excitation fluence (Mauzerall, 1976) and, thus, gives no information about the excitation migration parameters. In fact, the importance of this fluctuation effect was demonstrated from an analysis of fluo-

Received for publication 1 March 1995 and in final form 8 June 1995.

Address reprint requests to Dr. Leonas Valkunas, Institute of Physics, A. Gostauto 12, Vilnius 2600, Lithuania. Tel.: 3702-612610; Fax: 3702-617070; E-mail: valkunas@ktl.mii.lt.

© 1995 by the Biophysical Society

0006-3495/95/09/1117/13 \$2.00

rescence (Mauzerall, 1982) and charge separation (Mineev and Razjivin, 1987) experiments at high excitation intensities. The further development of the theory for bi-excitation annihilation in domains (Paillotin et al., 1979; Den Hollander et al., 1983), taking into account both the distribution of the fluctuations per domain and the annihilation decay rate, due to collisions of the two excitations in a molecular array (Suna, 1970) has demonstrated the competitive character of both processes. These theories subsequently have been used to analyze the intensity dependence of the fluorescence quantum yield of bacterial photosynthetic systems (Den Hollander et al., 1983; Bakker et al., 1983; Van Grondelle, 1985; Trinkunas and Valkunas, 1989), and the energy migration parameters at room temperature were determined. The conclusion is that energy migration occurs on a subpicosecond time scale and a hopping time τ_h of the excitation of the order of 0.5 ps was estimated. The estimation of the excitation migration radius, defined as $R = (z a^2 \tau / \tau_h)^{1/2}$ (here a is the lattice spacing, z is the coordination number, τ is the excitation lifetime), showed that the migration domain of the excitation during its lifetime (60 ps in the case of open RCs, see Timpmann et al., 1991) covers ~ 500 LHA molecules assuming a two-dimensional square lattice model. These results have been taken as evidence that the excitation trapping process is close to trap-limited, taking 24 pigment molecules (or 12 bacteriochlorophyll (Bchl) dimers) per RC, a typical size for the long-wavelength bacterial antenna.

This result contradicts the conclusion that the energy migration rate is slow (τ_h is of the order of 1–10 ps), which originates from the temperature dependence of the excitation decay kinetics at low-intensity excitation (Freiberg et al., 1989; Pullerits and Freiberg, 1991, 1992). However, these contradictions can be solved by assuming that two distance-scaling parameters are present in the system (Valkunas et al., 1992; Somsen et al., 1994). The first gives the average distance between neighboring pigments in the LHA, whereas the other reflects the mean distance to the RC. From the analysis of the available experimental results, it was concluded (Valkunas et al., 1992; Somsen et al., 1994) that the second scaling parameter is ~ 1.7 – 1.8 times the lattice spacing of the LHA (assuming a square lattice model for the LHA) and, therefore, the LHA can be treated as a supermolecule in the description of the low-intensity excitation decay.

The goal of this paper is to present a theory for the nonlinear excitation decay kinetics in a quasi-homogeneous photosynthetic antenna systems with emphasis on the correlative effects of excitations. It is evident that the annihilation kinetics is more sensitive to the variation of parameters under investigation than for instance the time-integrated fluorescence quantum yield. Other possible consequences affecting the nonlinear relaxation, namely, excitation correlations, local heating, the population of higher excited molecular states during the nonlinear annihilation and the excited state absorption, will also be discussed.

SINGLET-SINGLET ANNIHILATION

The starting point of our analysis is a system of M pigment molecules located on the sites of a lattice. Each molecule is characterized by the set of the singlet states S_0, S_1, \dots, S_n . Here we will consider the high temperature case where the inhomogeneous distribution of molecular states in the system can be neglected. The effect of inhomogeneous broadening further complicates the description of the annihilation process, and will be discussed below. Upon single-pulse excitation, the molecular transition $S_0 \rightarrow S_1$ is determined by the excitation rate $J(t)$ per molecule. Excitation of already excited molecules to a higher excited state occurs at the rate of $\alpha J(t)$ per molecule, or the $S_1 \rightarrow S_0$ transition will be stimulated at the rate $\bar{\alpha} J(t)$ (α and $\bar{\alpha}$ will be defined later). Because of diffusion, the excitations move on the lattice and, upon approaching one another, may annihilate according to the scheme shown in Fig. 1 *a*. Because of the process depicted in Fig. 1 *a* or by direct excitation of already excited molecules, at high excitation intensities a considerable population of higher excited states can be reached. Assuming that among the higher excited states S_2 has the longest lifetime, by a very similar annihilation mechanism as shown in Fig. 1 *a*, molecules in S_2 state may serve as mobile quenchers for S_1 excitations (Fig. 1 *b*) and vice versa (Fig. 1 *c*).

Because of the many-particle nature of the nonlinear annihilation process, a detailed description can be obtained by formulating a set of kinetic equations for the many-particle distribution functions (see Appendix). Suna (1970) was the first to apply such an approach to excitation annihilation in molecular crystals. Here we will generalize this approach for two types (S_1 and S_2) of singlet excitations on a finite network of molecules under intense pulse excitation.

Let us assume that the distributions of S_1 and, consequently, S_2 excitations are uniform. This may be realized in an experiment by choosing the correct excitation conditions. Then the kinetics of the corresponding densities of excitations n_1 and n_2 (by taking into account the natural normalization condition $n_0 + n_1 + n_2 = 1$, n_0 being the ground-

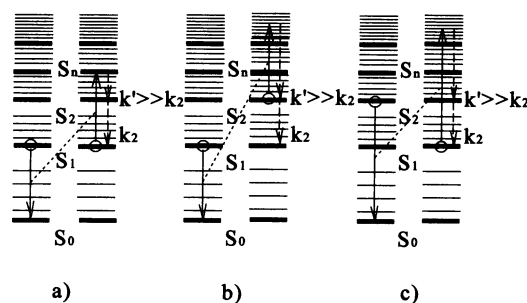


FIGURE 1 Singlet electronic and vibronic levels of pigment molecules, singlet-singlet annihilation scheme, and excitation paths involving two sorts of excitations. (*a*, *b*) S_1 - S_1 annihilation; (*c*) S_1 - S_2 annihilation. The excitation relaxation paths with rate constants k' and k_2 are also indicated in the scheme.

state population) is given by the following set of equations (see Appendix):

$$\frac{dn_1}{dt} = -[k_1(t) + (1 + \alpha + \bar{\alpha})J(t)]n_1 - 2\gamma(t)n_1^2 - \beta(t)n_1n_2 + [k_2 - J(t)]n_2 + J(t) \quad (1)$$

$$\frac{dn_2}{dt} = -k_2n_2 + \gamma(t)n_1^2 + \alpha n_1J(t), \quad (2)$$

where k_2 is the S_2 excitation lifetime and

$$k_1(t) = k + k_0[1 - \eta(t)] + k_c\eta(t). \quad (3)$$

k is the S_1 excitation relaxation rate in the system without RCs, k_0 and k_c are the excitation relaxation rates in the case of open and closed RCs, respectively. In Eq. 3 $\eta(t)$ is the fraction of closed RCs. The application of Eq. 3 implies that we are using the so-called lake model for energy transfer (Paillotin et al., 1983; Geacintov et al., 1984). The time dependence of $\eta(t)$ is given by

$$\eta(t) = Nk_0 \int_0^t [1 - \eta(t')]n_1(t') dt' + \eta(0). \quad (4)$$

Here N is the number of pigment molecules of the LHA per RC, $\alpha = \sigma_1/\sigma_0$, $\bar{\alpha} = \bar{\sigma}_1/\sigma_0$; σ_0 and σ_1 are the absorption cross-sections of molecules in S_0 and S_1 states, respectively, and $\bar{\sigma}_1$ is the cross section for stimulated emission from S_1 . $\gamma(t)$ and $\beta(t)$ define the rates of S_1 - $S_1 \rightarrow S_2$ and S_1 - $S_2 \rightarrow S_2$ annihilation processes, respectively (see Eqs. A4, A5, A9, and A10 in the Appendix), and are given by

$$\gamma(t) = \sum_{\mathbf{r}} \lambda(\mathbf{r})g(\mathbf{r}, t); \quad \beta(t) = \sum_{\mathbf{r}} \mu(\mathbf{r})h(\mathbf{r}, t), \quad (5)$$

where $g(\mathbf{r}, t)$ and $h(\mathbf{r}, t)$ are the two-particle correlation functions that describe the relative distribution of a pair of S_1 excitations and a pair of S_1 and S_2 excitations, respectively. $\lambda(\mathbf{r})$ and $\mu(\mathbf{r})$ define the annihilation rates, respectively, which in the case of the Förster-type interaction are given by

$$\lambda(\mathbf{r}) = k_n \left(\frac{R_1^0}{r} \right)^6; \quad \mu(\mathbf{r}) = k_n \left(\frac{R_2^0}{r} \right)^6, \quad (6)$$

where R_1^0 and R_2^0 are the Förster annihilation radii and k_n is the radiative relaxation rate. Values for the S_2 state cross sections σ_2 and $\bar{\sigma}_2$ are not known. Here we assume that these values are smaller than $\sigma_0 \approx \sigma_1$ and $\bar{\sigma}_1$, respectively, in the spectral region of the ground-state absorption. Taking further into account that the S_2 lifetime is much smaller than that of S_1 , the process of S_1 - S_1 annihilation will dominate strongly over S_1 - S_2 annihilation. To obtain the two-particle correlation functions $g(\mathbf{r}, t)$ and $h(\mathbf{r}, t)$ in Eq. 5, the following kinetic equations have to be solved (see Appendix):

$$\frac{\partial g(\mathbf{r}, t)}{\partial t} = 2D_1 \nabla_{\mathbf{r}}^2 g(\mathbf{r}, t) + H(g(\mathbf{r}, t)), \quad (7)$$

$$\frac{\partial h(\mathbf{r}, t)}{\partial t} = (D_1 + D_2) \nabla_{\mathbf{r}}^2 h(\mathbf{r}, t) + F(h(\mathbf{r}, t)), \quad (8)$$

where

$$H(g(\mathbf{r}, t)) = -2 \left[\lambda(\mathbf{r}) + \frac{J(t) + n_2[k_2 - J(t)]}{n_1} - J(t) \right] g(\mathbf{r}, t) + 2 \frac{J(t) + k_2 n_2 h(\mathbf{r}, t)}{n_1} \quad (9)$$

$$+ 2n_1 \left[2\gamma(t) - \sum_i [\lambda(\mathbf{l}) + \lambda(\mathbf{r} - \mathbf{l})] \frac{g(\mathbf{r}, \mathbf{l}, t)}{g(\mathbf{r}, t)} \right] g(\mathbf{r}, t) + n_2 \left[2\beta(t) - \sum_i [\mu(\mathbf{l}) + \mu(\mathbf{r} - \mathbf{l})] \frac{q(\mathbf{r}, \mathbf{l}, t)}{g(\mathbf{r}, t)} \right] g(\mathbf{r}, t),$$

and

$$F(h(\mathbf{r}, t)) = - \left[\mu(\mathbf{r}) + \frac{J(t) + n_2(k_2 - J(t))}{n_1} + J(t) \left(\alpha \frac{n_1}{n_2} - 1 \right) \right] h(\mathbf{r}, t) + \frac{J(t) + k_2 n_2 f(\mathbf{r}, t)}{n_1} + \frac{\alpha J(t) n_1 g(\mathbf{r}, t)}{n_2} - \frac{n_1^2}{n_2} \left[\gamma(t) - \sum_i \lambda(\mathbf{r} - \mathbf{l}) \frac{g(\mathbf{r}, \mathbf{l}, t)}{h(\mathbf{r}, t)} \right] h(\mathbf{r}, t) \quad (10)$$

$$+ n_1 \left[2\gamma(t) - 2 \sum_i \lambda(\mathbf{l}) \frac{q(\mathbf{r}, \mathbf{l}, t)}{h(\mathbf{r}, t)} \right] h(\mathbf{r}, t)$$

$$+ n_2 \left[\beta(t) - \sum_i \mu(\mathbf{l}) \frac{p(\mathbf{r}, \mathbf{l}, t)}{h(\mathbf{r}, t)} \right] h(\mathbf{r}, t);$$

and note that the solution of Eqs. 7 and 8 through Eqs. 9 and 10 implies that we have to know the three-particle correlation functions $g(\mathbf{r}, \mathbf{l}, t)$, $h(\mathbf{r}, \mathbf{l}, t)$, and $p(\mathbf{r}, \mathbf{l}, t)$, where $g(\mathbf{r}, \mathbf{l}, t)$ involves three S_1 excitations, $q(\mathbf{r}, \mathbf{l}, t)$ two S_1 and S_2 excitations, and $p(\mathbf{r}, \mathbf{l}, t)$ two S_2 and one S_1 excitations. $f(\mathbf{r}, t)$ in Eq. 10 defines the distribution function of a pair of S_2 excitations. The solution of Eqs. 7 and 8 in terms of series of kinetic equations for the multiple particle correlation functions is truncated after Eqs. 9 and 10 and implies that we will approximate the three-particle correlation functions as products of two-particle correlation functions (see below).

In Eqs. 7–10, D_1 and D_2 define the diffusion coefficients of S_1 and S_2 excitations, respectively, and D_1 is directly

connected with the excitation hopping time τ_h via the following relation: $D_1 = a^2/\tau_h$.

The initial conditions are given by

$$n_1(0) = n_2(0) = 0; \quad g(\mathbf{r}, 0) = h(\mathbf{r}, 0) = f(\mathbf{r}, 0) = 1, \quad (11)$$

and the following boundary conditions apply, which are obtained in a similar way as described by Gaididei et al. (1985):

$$\left. \frac{dg(\mathbf{r}, t)}{dt} \right|_{r=R_1} = \frac{2\Omega D_1}{R_1^2} \left. \frac{\partial g(\mathbf{r}, t)}{\partial r} \right|_{r=R_1} + H(g(\mathbf{r}, t))|_{r=R_1}; \quad (12)$$

$$\left. \frac{dh(\mathbf{r}, t)}{dt} \right|_{r=R_2} = \frac{2\Omega(D_1 + D_2)}{2R_2^2} \left. \frac{\partial h(\mathbf{r}, t)}{\partial r} \right|_{r=R_2} + F(h(\mathbf{r}, t))|_{r=R_2},$$

where Ω is the steric angle (for 3D systems $\Omega = 4\pi$, for 2D $- 2\pi$, for 1D $- 2$). These boundary conditions are obtained from Eq. 7 and 8 by rewriting them for two corresponding excitations separated by a distance equal to radius of the reaction spheres resulting in Eqs. 12. In Eq. 12, R_1 and R_2 represent the reaction radii, which will be defined below.

In the case of small domains, i.e., when the real radius of the system is much smaller than the excitation diffusion radius R (see Introduction), i.e.,

$$R = \sqrt{2dD_1/k_1}, \quad (13)$$

each domain can be approximated as a supermolecule in which the ultrafast energy migration does not play a role and for which the number of excitations in S_1 and S_2 are the only characteristics. Because of the very fast delivery of excitations to neighboring molecules, the time-dependent spatial distribution of the excitations within the domain does not play an essential role in solving Eqs. 7 and 8, and the annihilation processes is then limited by "static" annihilation between "nearest neighbors" according to the annihilation probabilities given in Eq. 6. A good approximation is then to assume that the annihilation rates $\gamma_{\text{stat}}(t)$ and $\beta_{\text{stat}}(t)$ are time-independent and the only statistical effects that are taken into account are those due to the initial distribution of the excitations over all of the domains. This is the basic approximation used by Paillot et al. (1979) and den Hollander et al. (1983).

For a diffusion-limited annihilation process, i.e., when the excitation diffusion radius (Eq. 13) is much smaller than the domain size, the annihilation rates (Eq. 5) are determined by the diffusion of the excitations toward the so-called "black sphere" of the reaction defined by the radii R_1 and R_2 for S_1 - S_1 and S_1 - S_2 annihilation, respectively (Ovchinnikov et al., 1989):

$$\gamma_{\text{dif}}(t) = \pi \frac{D_1}{(2R_1)^{d-1}} \left. \frac{\partial g(\mathbf{r}, t)}{\partial r} \right|_{r=R_1}; \quad (14)$$

$$\beta_{\text{dif}}(t) = \frac{\pi D_1 + D_2}{2 (2R_2)^{d-1}} \left. \frac{\partial h(\mathbf{r}, t)}{\partial r} \right|_{r=R_2};$$

where d is the dimension of the system, and the reaction radii R_1 and R_2 are determined via the following relations (Agranovich and Galanin, 1982):

$$\frac{R_1^2}{D_1} = \frac{1}{\lambda(R_1)}; \quad \frac{2R_2^2}{D_1 + D_2} = \frac{1}{\mu(R_2)}, \quad (15)$$

which by taking into account Eq. 6 and the Förster-type expression for D_1 , i.e., $D_1 = k_{\text{fl}}(R_0/a)^6 a^2$ results in the following expression for the reaction radius R_1 :

$$R_1 = \left(\frac{R_1^0}{R_0} \right)^{3/2} a. \quad (16)$$

For diffusion-limited annihilation, R_1 must be close to a , implying, according to Eq. 16 that $R_1^0 \approx R_0$. In the opposite case when $R_1 \gg a$, the static annihilation also must be taken into account. In that case, the following approximation can be used:

$$\gamma(t) = \gamma_{\text{dif}}(t) + \gamma_{\text{stat}}(t), \quad (17)$$

where $\gamma_{\text{dif}}(t)$ is defined according to Eq. 14 and $\gamma_{\text{stat}}(t)$ equals

$$\gamma_{\text{stat}}(t) = \int_0^{R_2} g_{\text{stat}}(\mathbf{r}, t) \lambda(\mathbf{r}) d\mathbf{r}, \quad (18)$$

where $g_{\text{stat}}(\mathbf{r}, t)$ is the solution of Eq. 7 in the static approximation within the sphere of reaction radius R_1 , i.e.,

$$\frac{\partial g_{\text{stat}}(\mathbf{r}, t)}{\partial t} = H(g_{\text{stat}}(\mathbf{r}, t)). \quad (19)$$

However, as it will become evident from the analysis of the difference spectra of photosynthetic membranes (see the following sections), $R_i^0 \leq R_0$ and, thus, for the systems with a size of the same order as the excitation diffusion radius (Eq. 13), the annihilation rate is determined by the excitation diffusion.

Let us discuss now qualitatively the time evolution of the kinetic equations (Eqs. 1-3). The stationary solution of these equations is given by

$$n_2 = \frac{J + n_1[J(\alpha - \bar{\alpha} - 1) - k_1]}{k_2 + J + \beta n_1}, \quad (20)$$

which is independent of $\gamma(t)$. From Eq. 20 it follows that at low excitation intensities where the nonlinearities can be neglected, $n_2 = 0$.

At high intensities where $n_2 \gg n_1$, but assuming that the following conditions $J \ll k_2$; $\beta n_1 \ll k_2$ are fulfilled, it follows that

$$n_2 \approx \frac{J}{k_2}. \quad (21)$$

The stationary solution of Eq. 2 then becomes

$$\gamma n_1^2 + J\alpha n_1 - J = 0. \quad (22)$$

Equations 21 and 22 are then valid at the time when the kinetic signals reflecting the populations n_1 and n_2 reach their maximum amplitude. For a description of the kinetics after the termination of the excitation pulse on a time scale slower than k_2^{-1} (implying that $dn_2/dt = 0$), it follows from Eq. 2 that

$$n_2 = \gamma(t) \frac{n_1^2}{k_2}, \quad (23)$$

and according to Eq. 1 the excitation decay kinetics is given by the following simplified equation:

$$\frac{d}{dt} n_1 = -k_1(t)n_1 - \gamma(t)n_1^2. \quad (24)$$

Thus, it follows that the effect due to the population of the S_2 state is only important during the action of the excitation pulse.

The time dependence of $\gamma(t)$ and $\beta(t)$ is determined by the correlation functions $g(\mathbf{r}, t)$ and $h(\mathbf{r}, t)$, respectively. The corresponding equations that describe the time evolution of these functions are in general very cumbersome and contain contributions of the three-particle correlation functions (see Eqs. 9 and 10). However, in the following section we will show that these terms can be greatly simplified during the rising part of the pulse (Agranovich and Efremov, 1980). If the following inequality is satisfied—

$$2n_1\gamma(t) + n_2\beta(t) < \lambda(\mathbf{r}) + \frac{J(t) + n_2[k_2 - J(t)]}{n_1} - J(t), \quad (25)$$

—then the nonlinear terms and the terms containing the three-particle correlation function in Eq. 9 can be neglected. By using Eq. 1, inequality (25) can be rewritten as

$$-\frac{1}{n_1} \frac{dn_1}{dt} < \lambda(\mathbf{r}) + k_1(t) + (\alpha + \bar{\alpha})J(t). \quad (26)$$

An analogous inequality can be obtained for the correlation function $h(\mathbf{r}, t)$:

$$-\left(\frac{1}{n_1} \frac{dn_1}{dt} + \frac{1}{n_2} \frac{dn_2}{dt}\right) < \mu(\mathbf{r}) + k_1(t) + (\alpha + \bar{\alpha})J(t). \quad (27)$$

Now it is evident that during the initial period when the

generation term is dominant, $(1/n_1)(dn_1/dt) > 0$ and $(1/n_2)(dn_2/dt) > 0$, the inequalities (26) and (27) are valid and, as a consequence, Eqs. 7 and 8 can be simplified in the following way:

$$\frac{dg(\mathbf{r}, t)}{dt} = 2D_1\nabla_r^2 g(\mathbf{r}, t) - 2\left[\lambda(\mathbf{r}) + 2\frac{J(t)}{n_1}\right]g(\mathbf{r}, t) + 4\frac{J(t)}{n_1}, \quad (28)$$

$$\frac{dh(\mathbf{r}, t)}{dt} = (D_1 + D_2)\nabla_r^2 h(\mathbf{r}, t) + 2\frac{J(t)}{n_1} + \alpha J(t)\frac{n_1}{n_2}g(\mathbf{r}, t) - \left[\mu(\mathbf{r}) + 2\frac{J(t)}{n_1} + J(t)\left(\alpha\frac{n_1}{n_2} - 1\right)\right]h(\mathbf{r}, t). \quad (29)$$

During the decay of the generation term, $(1/n_1)(dn_1/dt)$ and $(1/n_2)(dn_2/dt)$ change their signs, and inequalities (26) and (27) may no longer be true. The physical explanation for the simplification shown in Eqs. 28 and 29 is that during the random generation of the excitations in the domain, the correlations are continuously destroyed, whereas this is not the case when the generation is switched off.

When the excitation pulse is over, the excitation kinetics is determined by Eq. 24, and, therefore, we must consider the correlation function $g(\mathbf{r}, t)$, which then satisfies the following equation:

$$\frac{dg(\mathbf{r}, t)}{dt} = 2D_1\nabla_r^2 g(\mathbf{r}, t) - 2\lambda(\mathbf{r})g(\mathbf{r}, t) + \left[\gamma(t) - \sum_{\mathbf{r}'} [\lambda(\mathbf{r}') + \lambda(\mathbf{r} - \mathbf{r}')] \frac{g(\mathbf{r}, \mathbf{r}', t)}{g(\mathbf{r}, t)}\right]g(\mathbf{r}, t). \quad (30)$$

The three-particle correlation function $g(\mathbf{r}, \mathbf{r}', t)$ can be estimated by means of the Kirkwood approximation:

$$g(\mathbf{r}, \mathbf{r}', t) = g(\mathbf{r}, t)g(\mathbf{r}', t)g(\mathbf{r} - \mathbf{r}', t), \quad (31)$$

which is correct only at low excitation density n_1 . After substitution of Eq. 31 into Eq. 30 and developing $g(\mathbf{r} - \mathbf{r}')$ in a Taylor series in the point \mathbf{r} , Eq. 30 takes the following form:

$$\frac{dg(\mathbf{r}, t)}{dt} = 2D_1\nabla_r^2 g(\mathbf{r}, t) - 2\lambda(\mathbf{r})g(\mathbf{r}, t) + 2\gamma(t)n_1g(\mathbf{r}, t)[1 - g(\mathbf{r}, t)]. \quad (32)$$

Thus, a comprehensive set of kinetic equations is obtained, which is the basis for the analysis of the excitation decay kinetics following the action of high excitation intensities.

EXCITATION TRAPPING BY THE REACTION CENTER

Excitation trapping by the reaction center is described by Eq. 8, the solution of which is

$$\eta(t) = 1 - [1 - \eta(0)] \exp \left[-Nk_0 \int_0^t n_1(y) dy \right], \quad (33)$$

where the initial fraction of closed RCs $\eta(t)$ is given by the initial conditions. Thus, the temporal evolution of the fraction of closed reaction centers due to excitation trapping is determined by the excitation flux from the LHA to the RC.

If the excitation decay kinetics $n_1(t)$ can be approximated as a single-exponential, i.e., $n_1(t) \cong n_1(0)\exp(-kt)$, it follows from Eq. 33 that the excitation trapping rate equals $n_1(0)Nk_0$. Through the initial value $n_1(0)$, the trapping rate is proportional to the excitation intensity. Only when $n_1(0) \ll 1$ does the excitation trapping rate equal k . Therefore, only at low excitation intensities does an analysis of the $\eta(t)$ kinetics allow the determination of the excitation trapping rate. The process of excitation trapping after an intense laser flash competes with singlet-singlet annihilation, which is evident from multiple flash experiments with plants (Geacintov et al., 1984; Dobek et al., 1985). Similar experiments with bacteria (Bakker et al., 1983) have shown that using picosecond, intense laser pulses it is very difficult to convert all of the RCs into a closed state, demonstrating that even at medium high excitation intensities singlet-singlet annihilation is more effective than trapping.

Quantum yield of the excitation trapping $Q(z)$ equals $Q(z) = [\eta(\infty) - \eta(0)]/z$ by definition, where $z = \int J(t) dt/N$ is the number of excitations per RC. Thus, from Eq. 33 the ratio between the quantum yield of excitation trapping $Q(z)$ and the relative fluorescence quantum yield ϕ_f —this value equals 1 for annihilation-free conditions—can be calculated (Valkunas, 1989; Geacintov et al., 1984):

$$Q(z) = \frac{1}{z} [1 - \eta(0)] [1 - \exp(-Q_0 \phi_f z)], \quad (34)$$

where $Q_0 = k_0/(k_0 + k)$. It is evident that at low excitation intensities ($z \ll 1$) and in the case of open RCs ($\eta(0) = 0$) $Q(z) = Q_0$. (We note that the relationship between the fluorescence and trapping quantum yields given by Eq. 34 is a direct consequence of the lake model for the LHA (Den Hollander et al., 1983; Bakker et al., 1983; Valkunas, 1989; Geacintov et al., 1984). In the case of a puddle model, a relation similar to Eq. 34 can be obtained by replacing ϕ_f with 1 (Geacintov et al., 1984).)

Equation 34 is sensitive to N , the number of the LHA pigments per RC, i.e., it is dependent on the normalization of z . For instance, from the experimental data for *R. rubrum* (Bakker et al., 1983) where the intensity for which $zN_{RC} = 1$ (N_{RC} is the number of RCs per domain) is indicated (see Fig. 2), by applying Eq. 34 where $Q(z)$ becomes close to Q_0 , we obtain $N_{RC} = 20$ – 25 at room temperature.

At high excitation intensities, when $z \gg 1$, Eq. 34 gives $Q(z) = [1 - \eta(0)]/z$, i.e., the excitation trapping efficiency becomes independent of the structure and parameters of the LHA. This is the main reason why calculations based on the

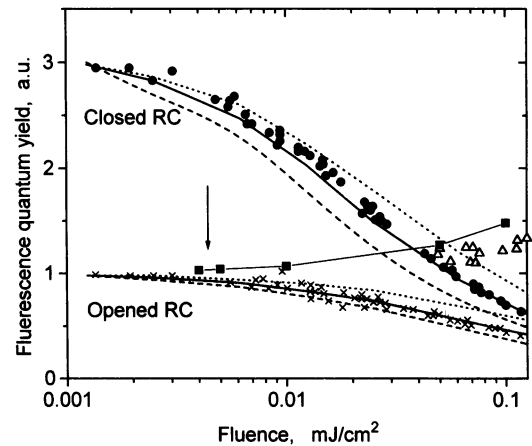


FIGURE 2 Fluorescence quantum yield dependencies on the excitation fluence in chromatophores. Experimental points (Bakker et al., 1983) are shown by crosses ("open RC") and filled circles ("closed RC"); open triangles show the fluorescence quantum yield Φ_f vs. state of the RC, i.e., η . Theoretical data (lines) are obtained for the diffusion-limited annihilation ($R_0^1 \cong R_0$) by numerical solutions of Eqs. 1–5 (32) using the initial and boundary conditions as expressed by Eqs. 11 and 12 and by neglecting the correlations between the excitations S_1 and S_2 . The chromatophore is assumed to be a sphere of radius $R = 10a$, a being the mean space between the pigments (see Trinkunas and Valkunas (1989) for details). The only fitting parameters are N , the number of Bchl molecules per RC and R_0 , the Förster migration radius. The former one ensures the correct ratio of the fluorescence quantum yield for initially open and closed RCs ($N = 12$), whereas the variation of R_0 (dotted line for $5.0a$, solid one for $5.5a$, and dashed for $6.0a$) matches the slope of experimental curves. Other parameters used in calculations: $k^{-1} = 3.5$ ns, $k_n^{-1} = 18$ ns, $k_0^{-1} = 60$ ps, $k_c^{-1} = 200$ ps, $k_2^{-1} = 1$ ps, $\tau_{\text{pulse}} = 35$ ps, $\alpha = \bar{a} = 1$. The arrow indicates the excitation intensity corresponding to one photon per domain, obtained from asymptotics of the RC charge separation quantum yield (\blacksquare), which was calculated from the experimental RC fluorescence quantum yield (Δ) by means of the following relation $\Phi_f = [1 - (k_0 - k_c)\eta/k_0]^{-1}$ (see Den Hollander et al., 1983).

excitation distribution statistics in the domain only (and not taking into account the actual dynamics of the processes under consideration) fit to the experimental data of Mineev and Razjivin (1987).

Equation 3 determines the average excitation trapping rate in a domain with open and closed RCs. The averaging procedure assumes that the state of a particular RC is independent of the state of other RCs or, in other words, the RCs are not combined into clusters in the domain. Therefore, the average or effective trapping rate in a domain containing such a mixture of open and closed traps is obtained by taking the sum of the excitation trapping rates for open (k_0) and closed (k_c) RCs multiplied by the relative probability to find the RC in each of these states, i.e., by $1 - \eta(t)$ and $\eta(t)$, respectively.

A final assumption in obtaining Eq. 3 is that the trapping is monoexponential. This is supported by calculations for two- and three-dimensional arrays of pigments assuming periodic boundary conditions and a homogeneous initial distribution of the excitation (Valkunas et al., 1986; Hemenger et al., 1972). Therefore, this assumption is consistent with the averaging procedure discussed above and

Eq. 3 can be used to describe intensity-dependent kinetics for systems containing one sort of LHA pigments and at high temperatures, where the spectral inhomogeneity of the LHA is not essential.

Our recent analysis of the temperature dependence of the excitation trapping by RCs has suggested that two distance-scaling parameters determine the organization of the LHA pigments: the pigment-pigment distance within the LHA and the pigment-RC distance (Valkunas et al., 1992; Somsen et al., 1994). It was concluded that the distance-scaling parameter from the LHA to the RC is ~ 1.7 times larger than the distance-scaling parameter within the LHA and, thus, the energy trapping rates k_0 and k_c are mainly limited by the slow rate of energy transfer from the nearest surrounding pigments to the RC. Also, in that case the monoexponential approximation for the kinetics of excitation trapping holds (Somsen et al., 1994; Valkunas et al., 1986). However, these differences in the distance-scaling parameters imply that the excitation equilibrates within the domain of the LHA before being trapped by the RC, and the kinetic processes taking place within the LHA become independent from the trapping processes. This implies that the singlet-singlet annihilation and trapping in fact probe different energy transfer steps.

TRANSIENT ABSORPTION AT VARIOUS EXCITATION INTENSITIES

When the change in optical density ΔA of a sample, $\Delta A \ll 1$, the difference absorption observed by a weak probe pulse, can be estimated from the following expression:

$$\Delta A(\lambda, t) = \frac{C\kappa}{\ln 10} \int I_p(t-t') \times \left[\sum_i n_i(t') \sigma_i(\lambda) - \sigma_0(\lambda) + \Delta A_{\text{corr}}(\lambda, t') \right] dt', \quad (35)$$

where λ and $I_p(t)$ are the wavelength and the pulse shape of the probing pulse, respectively, C is the concentration of pigment molecules in the sample with thickness κ , and $\Delta A_{\text{corr}}(\lambda, t)$ is the change in the difference spectrum due to the correlations between excitations, which is important at high excitation intensities. At low excitation intensities and if $\Delta A_{\text{corr}}(\lambda, t)$ can be neglected, Eq. 35 leads to the well known result that the value of $\Delta A(\lambda, t)$ is proportional to the convolution of the cross-correlation of the pump and probe laser pulses and the molecular response function. At high excitation intensities, when the exciton-exciton annihilation starts to contribute, the evolution of the difference spectra becomes much more complicated. The additional effect due to the correlation between the excitations can occur if the molecule that is excited in the near vicinity of another excited molecule and, thus, due to the dispersion-like interaction between

both excitations the ground-state absorption of the molecule σ_0 or the excited-state spectra σ_1 are changed. This effect is included into the term $\Delta A_{\text{corr}}(\lambda, t)$, i.e.,

$$\Delta A_{\text{corr}}(\lambda, t) = n_1 \sum_r [\sigma_0^r(\lambda) - \sigma_0(\lambda)] + n_1^2 \sum_r g(r, t) \times \left[\sum_{r'} [\sigma_0^{r,r'}(\lambda) - \sigma_0(\lambda)] + \sigma_1^r(\lambda) - \sigma_1(\lambda) \right], \quad (36)$$

where the sum over r goes over all molecules at the distance r , $\sigma_0^r(\lambda)$ is the ground-state absorption ($i = 0$) and excited-state absorption and stimulated emission ($i = 1$) cross sections of the molecule, which is situated close to the excited molecule at the distance r , and $\sigma_0^{r,r'}(\lambda)$ is the ground-state absorption of the molecule situated close to two excited molecules. In the case where there is no correlative effect on the ground- and excited-state absorption, i.e., $\sigma_0^r(\lambda) = \sigma_0(\lambda)$ and $\sigma_1^r(\lambda) = \sigma_1(\lambda)$ the time dependence of the difference spectra displays the excitation annihilation kinetics only. First, we will consider the dependence of the maximum value of the absorption difference spectra on the excitation intensity assuming that the correlative effects are absent. Then we will discuss the correlative effect on the difference spectra below. The stationary solution of the kinetic Eqs. 1 and 2 that leads to Eq. 21 in the case of very high intensities, when $n_2 \gg n_1$, can be rewritten as Eq. 22. In that case and for "broad" pulses, i.e., when $J_0 \tau_{\text{pulse}} > n_1 + n_2$ (τ_{pulse} is the pulse duration), Eq. 22 is valid during the excitation pulse and, thus,

$$\sum_i n_i(t) \sigma_i(\lambda) - \sigma_0(\lambda) = n_2(t) [\sigma_2(\lambda) - \sigma_0(\lambda)]. \quad (37)$$

Using Eqs. 21 and 37 and assuming the pump and probe pulses are Gaussian, the maximal value of the spectral changes is given by

$$\Delta A^{\text{max}}(\lambda) = \frac{J_0 A(\lambda)}{\sqrt{2} k_2 \tau_{\text{pulse}} \sigma_0(\lambda)} [\sigma_2(\lambda) - \sigma_0(\lambda)], \quad (38)$$

where J_0 is the maximal value of the excitation pulse and $A(\lambda) = C\kappa\sigma_0(\lambda)/\ln 10$ is the absorbance of the sample. As mentioned above, at low excitation intensities, i.e., when $n_1 \gg n_2$, $\Delta A(\lambda, t)$ is given by

$$\Delta A(t, \lambda) = \frac{A(\lambda)}{\sigma_0(\lambda)} n_1(t) [\sigma_1(\lambda) - \sigma_0(\lambda)]. \quad (39)$$

To obtain the maximal value of ΔA , the stationary value of n_1 obtained from Eq. 1 has to be substituted into Eq. 39.

The absorption spectrum $\sigma_2(\lambda)$ is a continuous function of λ , and here we assume that it does not contain pronounced features in the spectral region of the ground-state absorption. Thus, according to Eq. 38, the difference spectrum reflects the bleaching of the ground-state absorption $\sigma_0(\lambda)$ of the antenna pigments. This is indeed observed in experiments (Borisov et al., 1982, 1984) with the purple photosynthetic bacterium *Rs. rubrum* at very high excitation conditions. Another consequence of Eq. 38 is the linear

dependence on the excitation intensity. Moreover, the slope of this linear dependence is directly connected with k_2 , the excitation relaxation rate from the higher excited state S_2 . The experimental results obtained by Borisov et al. (1982) demonstrate the linear dependencies (see Fig. 3) and, from this data, k_2 is estimated to be of the order of 1 ps^{-1} . A measurable excitation of S_2 state occurs only during the action of the excitation pulse and, as it follows from Eq. 23, its value becomes small because of the fast relaxation rate k_2 . Thus, the difference spectrum (38) obtained at high excitation intensities is transformed after the termination of the excitation pulse into the spectrum (Eq. 39), which evolves with the time dependence of $n_1(t)$ according to Eq. 24. A similar interpretation was earlier presented by Kudzmauskas et al. (1985, 1986) to explain the spectral changes at high excitation intensities experimentally observed by Borisov et al. (1982, 1984).

Let us now return to the spectral changes determined by the correlations of excitations according to Eq. 36. The absorption cross section of the molecules situated in the vicinity of the excited molecule $\sigma_i^r(\lambda) = \sigma_i^r(\omega)$ and $\sigma_0^{r'}(\lambda) = \sigma_0^{r'}(\omega)$ can be estimated as follows:

$$\sigma_i^r(\omega) = \sigma_i[\omega - \omega_i - \hbar^{-1}V_i(\mathbf{r})], \quad (40)$$

$$\sigma_0^{r'}(\omega) = \sigma_0[\omega - \omega_0 - \hbar^{-1}V_0(\mathbf{r}') - \hbar^{-1}V_0(\mathbf{r} - \mathbf{r}')],$$

where $\sigma_i(\omega - \omega_i) = \sigma_i(\lambda)$ is the homogeneously broadened absorption of pigments in the i th state with the absorption at ω_i and $V_i(\mathbf{r})$ determines the correlative interaction between two excited molecules at a distance r from each other, i.e.,

$$V_i(\mathbf{r}) = V_i(\mathbf{a})\left(\frac{a}{r}\right)^n, \quad (41)$$

where $V_i(\mathbf{a})$ is the value of such an interaction between "nearest-neighbors" and the power-law (n) is determined by

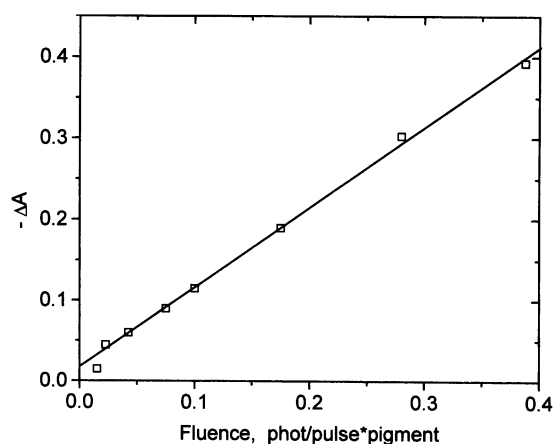


FIGURE 3 Change in absorption at 880 nm in chromatophores of *R. rubrum* as a function of the excitation fluence (high excitation conditions). (□) Experimental points from Borisov et al. (1982) ($A(\lambda = 890 \text{ nm}) = 1$; $\tau_{\text{pulse}} = 25 \text{ ps}$). The slope of the solid line calculated according to Eq. 38 corresponds to $k_2 \approx 3.3 \text{ ps}^{-1}$.

the order of the multipole intermolecular interaction. For instance, in the case of dipole-dipole type interaction $n = 3$ (Davydov, 1971). Thus, it is evident that a significant deviation of $\sigma_i^r(\lambda)$ from $\sigma_i(\lambda)$ occurs only at small r when $r < r_i$, where the latter value is determined by the following equality:

$$\sigma_i^r(\lambda) = \sigma_i(\lambda). \quad (42)$$

Thus, the largest spectral changes due to correlative effects are obtained for those molecules that are closest in distance and according to the definition of the reaction radius R_1 (see Eq. 16), the correlation function can be considered in the static approximation (19). During the action of the excitation pulse, inequality (26) is fulfilled and, thus, the terms due to the three-particle correlations in Eq. 19 can be neglected, yielding the following stationary solution of Eq. 19:

$$g_{\text{stat}}(\mathbf{r}) = \frac{J}{n_1} \left[\lambda(\mathbf{r}) + \frac{J}{n_1} \right]^{-1}. \quad (43)$$

According to Eq. 22, the ratio J/n_1 increases with increasing excitation intensity and, thus, at the most high intensities g_{stat} approaches unity.

The kinetics of the static correlation function after the pulse action (neglecting the higher correlations) gives the following analytical expression:

$$g_{\text{stat}}(\mathbf{r}, t) = e^{-2\lambda(\mathbf{r})t}. \quad (44)$$

Thus, because of correlative effects induced during the action of the excitation pulse, a fast kinetic component may be observed, determined by Eq. 44. The kinetics is faster than the decay of n_1 , which occurs on the time scale of γ . Therefore, the spectral changes at high excitation intensities that arise either from the population of higher excited states or from the correlative effects (in the static approximation) are indistinguishable. Both introduce fast kinetics and, according to Eqs. 21 and 22, both are proportional to J . The spectral changes that remain after the excitation pulse are determined mainly by the population of the first excited states of pigment molecules (Eq. 39). In that case the spectral difference of $\sigma_0^r(\lambda)$ and $\sigma_0(\lambda)$ is negligible, which implies that we can ignore the contribution of ΔA_{corr} . Then the single undefined parameter $\sigma_1(\lambda)$, which is contained in Eq. 39, can be determined from an analysis of the difference spectra at low excitation conditions:

$$\sigma_1(\lambda) = \frac{\Delta A(\lambda)\sigma_0(\lambda)}{n_1 A(\lambda)} + \sigma_0(\lambda). \quad (45)$$

It is evident that $\sigma_1(\lambda)$ describes the optical transitions from the S_1 state to higher excited states ($\sigma_1 = \alpha\sigma_0$) as well as the stimulated emission $\bar{\alpha}\sigma_0$. Using Eq. 45, we have analyzed the experimental results obtained for *R. rubrum* (Nuijts et al., 1985) assuming that $N = 50$. From this analysis, we obtain the spectrum presented in Fig. 4 (open diamonds). This spectrum shows a strong negative contribution on the

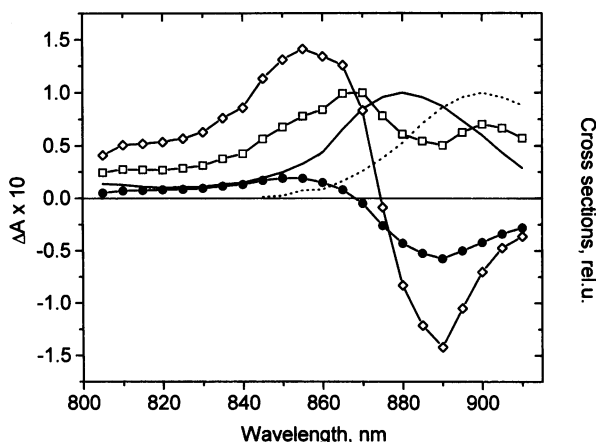


FIGURE 4 S_1 state absorption cross section estimated for two different concentrations of excitations. (\diamond , cross sections estimated according to Eq. 45 by using the measured difference absorption spectrum of chromatophores (\bullet , Nuijs et al. (1985), $A(\lambda = 532 \text{ nm}) = 0.31$; excitation fluence = 1 phot/RC pulse); \square , cross sections obtained by assuming a fourfold higher excitation concentration. The solid line represents the ground-state absorption cross section, and the dotted line represents the stimulated emission cross section.

long-wavelength side. If correct, this spectrum directly shows that the excited molecule strongly perturbs the ground-state absorption spectrum of the neighboring pigment molecules, i.e., the correlative effects in the spectral changes as described by the first term in Eq. 36, are indeed present.

However, it is now apparently believed that the photosynthetic unit of *Rs. rubrum* contains 24 Bchls/RC and, moreover, that these are probably arranged as dimers. Thus, by renormalizing the intensity scale yields an estimate of $\sigma_1(\lambda)$ as is depicted in Fig. 4 (*open squares*). Probably, the peak at 868 nm reflects the excited state absorption, i.e., due to $S_1 \rightarrow S_n$ transitions, within a single dimer (van Grondelle et al., 1994). On the other hand, it is noteworthy that the spectrum of $\alpha\sigma_0(\lambda)$ resembles the analogous spectrum of Bchl molecules in polar solvents (Becker et al., 1991).

ANNIHILATION KINETICS IN PHOTOSYNTHETIC MEMBRANES

From the spectrum of $\sigma_1(\lambda)$ obtained in the previous section, we can estimate the values of the Förster radii R_1^0 and R_0 . Inspection of Fig. 4 shows that spectral overlap of the fluorescence spectrum with the absorption spectra $\sigma_0(\lambda)$ and $\sigma_1(\lambda)$ is very similar and directly indicates that the ratio of these radii, i.e., R_1^0/R_0 , must be close to unity. Thus, according to Eq. 16 the “black sphere” radius R_1 equals a and, therefore, the annihilation process is purely diffusion-limited. This is an essential simplification of the theoretical analysis of singlet-singlet annihilation, because only two semiempirical parameters are left in the fitting procedure of the experimental data, namely, D_1 (or τ_h) and N .

The annihilation kinetics have been analyzed using the two-dimensional “bubble” model of the domain, i.e., assuming that pigment molecules are situated on the surface of a sphere. The number of RCs in a domain was calculated from an analysis of fluorescence quantum yield as a function of total laser energy (see Fig. 2 of Trinkunas and Valkunas, 1989), and it was concluded that $\tau_h = 0.65 \text{ ps}$ and $N = 12$ (or even less). Taking into account that the LHA of *Rs. rubrum* contains 24 Bchls/RC, this implies that the main “building blocks” are at least dimers. Also, a detailed spectroscopic analysis of the B820 subunit of the LHA of *Rs. rubrum* and the intact LHA has indicated strongly that the basic functional unit is a dimer of Bchl *a* (Visschers et al., 1991; Van Mourik et al., 1992; van Grondelle et al., 1994). It is noteworthy that the fluorescence quantum yield analysis is not sensitive to a variation in the size of the domain. This is in contrast to the annihilation rate time dependence, $\gamma(t)$ (see Fig. 5), which is due to the correlative effects in the excitation dynamics. The smaller the system, the higher the sensitivity to these correlative effects. It is evident that in large domains, within the lifetime of the excitation, the excitation annihilation can be well approximated by $\gamma = \text{const.}$, which is only true in three-dimensional systems of infinite size according to the general theory (Ovchinnikov et al., 1989). The approximation $\gamma = \text{const.}$ can be used to fit the excitation kinetics in RC-less chromatophores of *Rs. rubrum* at low excitation intensities ($J_0 < 0.025$ photons/Bchl pulse), as is demonstrated in Fig. 6. Assuming $\gamma = \text{const.}$ and analyzing the annihilation kinetics at moderate excitation intensities (see Fig. 7) yields the same value for N ($N = 12$) and τ_h ($\tau_h = 0.65 \text{ ps}$), as obtained from the analysis of the total fluorescence quantum yield. Note, however, that the resulting kinetics are sensitive to variations in the numerical values of these parameters, as demonstrated in Fig. 8. Also, the occupation of the higher excited states, S_2 (or spectral changes due to correlations between excitations), must explicitly be taken into account. The effects due to correlations between excitations, which

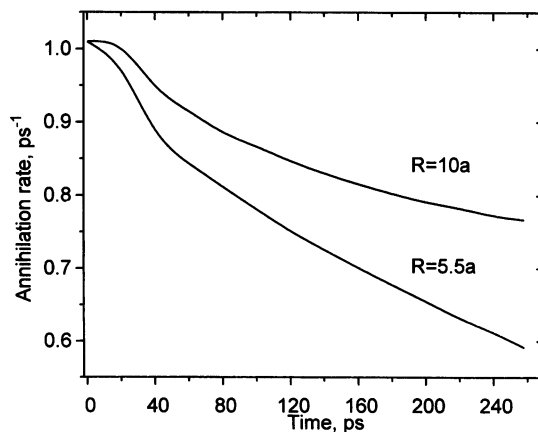


FIGURE 5 Time course of annihilation rate. R stands for the radius of the chromatophore. Excitation fluence = 0.65 phot/RC pulse, $\eta = 1$; $R_0 = 5.5a$; the remaining parameters are the same as those used in Fig. 2.

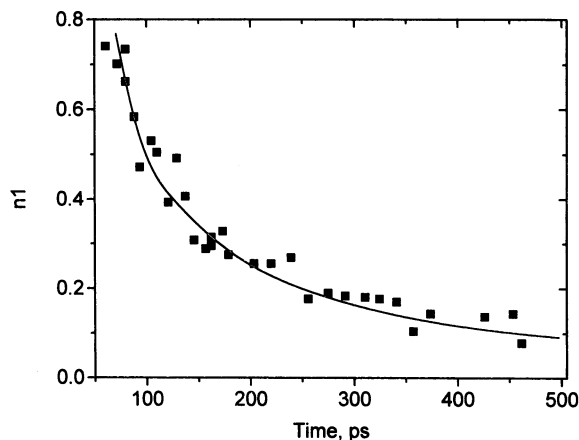


FIGURE 6 Excitation decay kinetics in the RC-less mutant to the photosynthetic bacterium *R. rubrum*. (■) Experimental points (Danielius et al., 1986); (—) calculation according to Eq. 1 and neglecting excitation correlations with annihilation rate constant $\gamma = 1 \text{ ps}^{-1}$, $k_1(t) = k$, and the other parameters are the same as those used in Fig. 2.

are displayed via the time-dependence of γ , can be observed at high excitation intensities. Qualitatively, this effect is evident from the experimental data (Borisov et al., 1984), which indicate that the excitation kinetics after normalization is independent of the excitation intensity. Here it is shown that after the termination of the excitation pulse, the amount of excitations that remains in the domain is the same. There are several possible explanations for this, which we will mention shortly: 1) increasing the temporal dependence of γ , 2) taking into account the occupation of higher excited states S_2 , 3) by including spectral changes due to the higher correlations between the excitations, and 4) by increasing the local temperature due to the stimulated

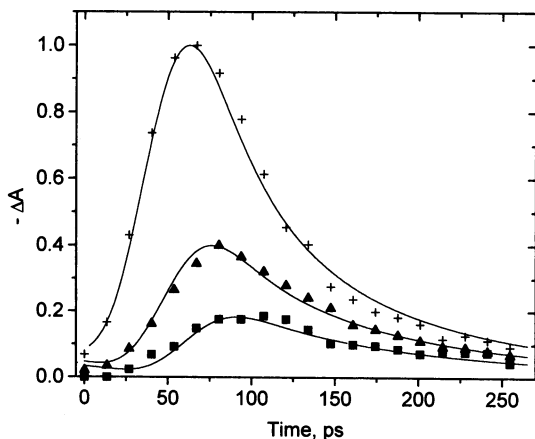


FIGURE 7 Comparison of the model kinetics calculated according to Eqs. 1 and 2 with the Förster annihilation radius $R_0 = 5.5a$ ($a = 20 \text{ \AA}$, the other parameters are as indicated in Fig. 2) to the experimental kinetics curves (Nuijs et al., 1985) at different excitation fluences: (■) 0.031 mJ/cm^2 (0.12 phot/RC), (▲) 0.081 mJ/cm^2 (0.32 phot/RC), and (+) 0.34 mJ/cm^2 (1.4 phot/RC).

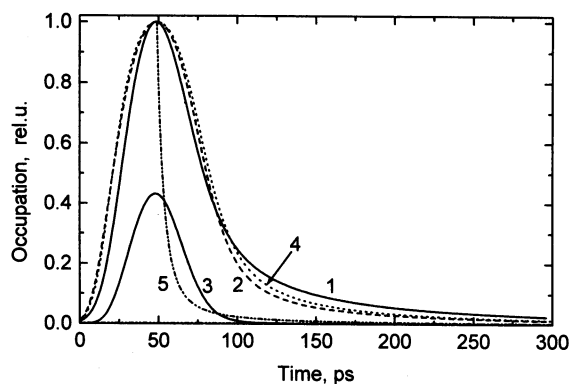


FIGURE 8 Simulation of the excitation decay at various excitation intensities according to Eqs. 1–3. Kinetic traces 1 and 2 calculated for occupation of state S_1 do not show significant differences despite the excitation fluences J_0 differ by one order of magnitude: 0.5 and 5.0 photon/pulse per pigment, respectively. Trace 3 is for occupation of state S_2 . Trace 4 is calculated with annihilation rate $\gamma = 0.5 \text{ ps}^{-1}$ (compare with $\gamma(t)$ in Fig. 5 for $R = 10a$) and neglecting the S_2 state occupation. Trace 5 is obtained for $\delta(t)$ pulse excitation with the same conditions as for trace 4. Curves 3–5 are calculated for $J_0 = 5.0$ photon/pulse per pigment. Other parameters are as follows: $k_c^{-1} = 200 \text{ ps}$, $k_2^{-1} = 1 \text{ ps}$, $\eta = 1$, $\tau_{\text{pulse}} = 35 \text{ ps}$, $N = 12$.

relaxation process that occurs during singlet-singlet annihilation (Valkunas et al., 1991; Gulbinas, 1994). The consequences of most of these effects are demonstrated in Fig. 8.

FINAL REMARKS

We conclude that the transient spectra obtained at high excitation intensities exhibit specific spectral changes which are evident during the initial stage after the pulse. These include 1) spectral changes due to the occupation of higher excited states (see Eqs. 38) and 2) spectral changes due to the correlation between excitations (see Eq. 36). The possibility to create excitations in higher excited states during singlet-singlet annihilation was demonstrated in the anthracene crystal at room temperature by Katoh and Kotani (1993). However, spectral effects due to the correlative behavior of excitations can compete with those due to occupation of higher excited states. Therefore, special comparative fluorescence and absorption measurements should be carried out. The transient spectra exhibit the effects of the changes in the ground-state absorption $\sigma_0^T(\lambda)$, whereas the fluorescence kinetics only shows the correlative spectral changes in the excited-state $\sigma_1^T(\lambda)$.

It is noteworthy that the high-excitation intensity stimulates the heating of the local surrounding of the pigment molecules, which can also disturb the transient spectra (Valkunas et al., 1991; Gulbinas et al., 1994). This effect is distinguishable in the transient spectra but not in the fluorescence kinetics, and the corresponding spectral changes are proportional to $\sigma_0^T(\lambda) - \sigma_0(\lambda)$, where $\sigma_0^T(\lambda)$ is the ground-state absorption of pigments at temperature T (heated surrounding). The relaxation rate of

these spectral changes is determined by the heat exchange with the thermostat, i.e., with energy relaxation into other vibrational modes or with the heat diffusion into more distant parts of the protein or into the solvent. Thus, the comparative analysis of transient spectra and the fluorescence kinetics provides information about the rates of heat relaxation. As was demonstrated by Gulbinas et al. (1994), the heat relaxation kinetics in some molecular

aggregates is longer than the relaxation of the electronic excitations and, thus, the former determines the long-term changes observed in the transient spectra.

The research described in this publication was made possible in part by grant No. LE 6000 from the International Science Foundation, the Dutch Foundation for Life Sciences (SLW), EC-grant CT 930278, and NATO Collaborative research grant 940851.

APPENDIX

To derive the kinetic equations (1–4), we introduce the distribution function $P_{N=N_1+N_2}^M(\mathbf{r}_1, \mathbf{r}_2, \dots, \mathbf{r}_{N_1}; \mathbf{r}'_1, \mathbf{r}'_2, \dots, \mathbf{r}'_{N_2})$ of the probability to find the system of M molecules containing N_1 molecules with the coordinates $\mathbf{r}_i, i = 1, \dots, N_1$ in the excited-state S_1 and N_2 molecules with the coordinates $\mathbf{r}'_j, j = 1, \dots, N_2$ in the excited state S_2 . The function P_N^M is normalized as follows:

$$\sum_{N=0}^M \sum_{N_1=0}^N \frac{1}{N_1! N_2!} \sum_{\{\mathbf{r}\}^{N_1} \cap \{\mathbf{r}'\}^{N_2} = \emptyset} P_N^M(\{\mathbf{r}\}^{N_1}; \{\mathbf{r}'\}^{N_2}) = 1, \quad (\text{A1})$$

where $\{\mathbf{r}\}^N \ni \mathbf{r}_1, \mathbf{r}_2, \dots, \mathbf{r}_N$. For compactness of the presentation the time is omitted in the list of arguments of function P_N^M . Assuming detailed balance for the probability distribution yields Eq. A2.

$$\begin{aligned} \frac{\partial}{\partial t} P_N^M(\{\mathbf{r}\}^{N_1}; \{\mathbf{r}'\}^{N_2}) = & \left(D_1 \sum_{i=1}^{N_1} \nabla_{\mathbf{r}_i}^2 + D_2 \sum_{j=1}^{N_2} \nabla_{\mathbf{r}'_j}^2 \right) P_N^M(\{\mathbf{r}\}^{N_1}; \{\mathbf{r}'\}^{N_2}) \\ & + J(t) \left[\sum_{\mathbf{r}_{N_1+1}} \left(\alpha \sum_{i=1}^{N_2} P_N^M(\{\mathbf{r}\}^{N_1+1}; \{\mathbf{r}'\}_i^{N_2}) \delta(\mathbf{r}_{N_1+1}, \mathbf{r}'_i) + \bar{\alpha} P_N^M(\{\mathbf{r}\}^{N_1+1}; \{\mathbf{r}'\}^{N_2}) \right) \right. \\ & \quad \left. + \sum_{i=1}^{N_1} P_{N-1}^M(\{\mathbf{r}\}_i^{N_1}; \{\mathbf{r}'\}^{N_2}) - (1 + \alpha + \bar{\alpha}) N_1 P_{N+1}^M(\{\mathbf{r}\}^{N_1}; \{\mathbf{r}'\}^{N_2}) \right] \\ & + k_1(t) \left(\sum_{\mathbf{r}_{N_1+1}} P_{N+1}^M(\{\mathbf{r}\}^{N_1+1}; \{\mathbf{r}'\}^{N_2}) - N_1 P_N^M(\{\mathbf{r}\}^{N_1}; \{\mathbf{r}'\}^{N_2}) \right) \\ & + k_2 \left(\sum_{\mathbf{r}_{N_2+1}} \sum_{i=1}^{N_1} P_N^M(\{\mathbf{r}\}^{N_1}; \{\mathbf{r}'\}^{N_2+1}) \delta(\mathbf{r}_i, \mathbf{r}'_{N_2+1}) - N_2 P_N^M(\{\mathbf{r}\}^{N_1}; \{\mathbf{r}'\}^{N_2}) \right) \\ & + \frac{1}{2} \sum_{\mathbf{r}_{N_1+1}, \mathbf{r}'_{N_2+2}} P_{N+1}^M(\{\mathbf{r}\}^{N_1+2}; \{\mathbf{r}'\}^{N_2-1}) [\delta(\mathbf{r}_{N_1+1}, \mathbf{r}'_{N_2}) + \delta(\mathbf{r}_{N_1+2}, \mathbf{r}'_{N_2})] \lambda (\mathbf{r}_{N_1+1} - \mathbf{r}_{N_1+2}) \\ & - 2 \sum_{j>i=1}^{N_1} P_N^M(\{\mathbf{r}\}^{N_1}; \{\mathbf{r}'\}^{N_2}) \lambda (\mathbf{r}_i - \mathbf{r}_j) + \sum_{\mathbf{r}_{N_1+1}} \sum_{i=1}^{N_2} P_{N+1}^M(\{\mathbf{r}\}^{N_1+1}; \{\mathbf{r}'\}_i^{N_2}) \mu (\mathbf{r}_{N_1+1} - \mathbf{r}'_i) \\ & - \sum_{i=1}^{N_1} \sum_{j=1}^{N_2} P_N^M(\{\mathbf{r}\}^{N_1}; \{\mathbf{r}'\}^{N_2}) \mu (\mathbf{r}_i - \mathbf{r}'_j). \end{aligned} \quad (\text{A2})$$

The first term on the right side of Eq. A2 determines the increase in the probability due to the excitation diffusion. The next term (between brackets) reflects the generation of excitations. The terms multiplied by k_1 and k_2 arise from excitation monomolecular decay and trapping. The next terms multiplied by the annihilation probabilities λ and μ represent the loss of excitations due to annihilation. Here it is assumed that because of the pairwise excitation collision, the double excited state is produced (see Fig. 1), which in a very short time relaxes to the state S_1 resulting in the loss of only one excitation of the pair.

To account for the lowest-order excitation correlations, the excitation probability distribution functions have to be averaged as follows:

$$f_{n=i+j}(\mathbf{r}_1, \dots, \mathbf{r}_i; \mathbf{r}'_1, \dots, \mathbf{r}'_j) = \sum_{N=n}^M \sum_{N_1=i}^{N-j} \frac{1}{(N_1 - i)! (N_2 - j)!} \frac{1}{\sum_{\{\mathbf{r}\}_{1, \dots, i}^{N_1} \cap \{\mathbf{r}'\}_{1, \dots, j}^{N_2} = \emptyset} P_N^M(\{\mathbf{r}\}^{N_1}; \{\mathbf{r}'\}^{N_2})}. \quad (\text{A3})$$

The semicolon in the parenthesis on the left side separates the coordinates of the molecules in the excited states S_1 (on the left) and S_2 (on the right). The kinetic equations for the n -particle distribution functions f_n are then obtained by a direct summation of Eq. A2 using Eq. A3. The expressions that one then obtains for the one-particle as well as two-particle excitation distribution functions are presented below.

$$\begin{aligned} \frac{\partial}{\partial t} f_1(\mathbf{r}_1;) &= [D_1 \nabla_{\mathbf{r}_1}^2 - k_1(t) - (\alpha + \bar{\alpha})J(t)] f_1(\mathbf{r}_1;) + k_2 f_1(\mathbf{r}_1) + J(t) f_1^0 \\ &\quad - 2 \sum_{\mathbf{r}_2} \lambda(\mathbf{r}_1 - \mathbf{r}_2) f_2(\mathbf{r}_1, \mathbf{r}_2;) - \sum_{\mathbf{r}'_2} \mu(\mathbf{r}_1 - \mathbf{r}'_2) f_2(\mathbf{r}_1; \mathbf{r}'_2), \end{aligned} \quad (\text{A4})$$

$$\frac{\partial}{\partial t} f_1(; \mathbf{r}'_1) = [D_2 \nabla_{\mathbf{r}'_1}^2 - k_2] f_1(; \mathbf{r}'_1) + \alpha J(t) f_1(\mathbf{r}_1;) + \sum_{\mathbf{r}_1} \lambda(\mathbf{r}_1 - \mathbf{r}'_1) f_2(\mathbf{r}_1, \mathbf{r}'_1;), \quad (\text{A5})$$

$$\begin{aligned} \frac{\partial}{\partial t} f_2(\mathbf{r}_1, \mathbf{r}_2;) &= [D_1 (\nabla_{\mathbf{r}_1}^2 + \nabla_{\mathbf{r}_2}^2) - 2(\alpha + \bar{\alpha})J(t) - 2k_1(t) - 2\lambda(\mathbf{r}_1 - \mathbf{r}_2)] f_2(\mathbf{r}_1, \mathbf{r}_2;) + J(t) [f_1(\mathbf{r}_1;) + f_1(\mathbf{r}_2;)] \\ &\quad + k_2 [f_2(\mathbf{r}_1; \mathbf{r}_2) + f_2(\mathbf{r}_2; \mathbf{r}_1)] - 2 \sum_{\mathbf{r}_3} [\lambda(\mathbf{r}_1 - \mathbf{r}_2) + \lambda(\mathbf{r}_2 - \mathbf{r}_3)] f_3(\mathbf{r}_1, \mathbf{r}_2, \mathbf{r}_3;) \\ &\quad + \sum_{\mathbf{r}'_1} [\mu(\mathbf{r}_1 - \mathbf{r}'_1) + \mu(\mathbf{r}_2 - \mathbf{r}'_1)] f_3(\mathbf{r}_1, \mathbf{r}_2; \mathbf{r}'_1), \end{aligned} \quad (\text{A6})$$

$$\begin{aligned} \frac{\partial}{\partial t} f_2(\mathbf{r}_1; \mathbf{r}'_1) &= [D_1 \nabla_{\mathbf{r}_1}^2 + D_2 \nabla_{\mathbf{r}'_1}^2 - \mu(\mathbf{r}_1 - \mathbf{r}'_1) - k_1(t) - k_2 - (\alpha + \bar{\alpha})J(t)] f_2(\mathbf{r}_1; \mathbf{r}'_1) + J(t) [\alpha f_2(\mathbf{r}_1, \mathbf{r}'_1;) + f_1(; \mathbf{r}'_1)] \\ &\quad + k_2 f_2(\mathbf{r}_1, \mathbf{r}'_1) + \sum_{\mathbf{r}_2} \lambda(\mathbf{r}_1 - \mathbf{r}_2) [f_3(\mathbf{r}_1, \mathbf{r}_2, \mathbf{r}'_1;) - 2f_3(\mathbf{r}_1, \mathbf{r}_2; \mathbf{r}'_1)] - \sum_{\mathbf{r}'_2} \mu(\mathbf{r}_1 - \mathbf{r}'_2) f_3(\mathbf{r}_1; \mathbf{r}'_2, \mathbf{r}'_1). \end{aligned} \quad (\text{A7})$$

The function f_1^0 in Eq. A4 determines the probability of single molecule to be in the ground state S_0 because it follows from Eq. A1 if the sum over the excited molecules is taken to $M - 1$.

In the case of homogeneous excitation conditions and taking into account the local character of the excitation trapping, the excitation distribution is thought to be homogeneous:

$$f_1^0 \equiv n_0, \quad f_1(\mathbf{r}_1;) \equiv n_1, \quad f_1(; \mathbf{r}'_1) \equiv n_2, \quad (\text{A8})$$

n_1 being density of the molecule in the state S_1 ($n_0 + n_1 + n_2 = 1$). Equations 1–5 are then obtained by introducing the relative distribution functions

$$g(\mathbf{r}_1 - \mathbf{r}_2) = f_2(\mathbf{r}_1, \mathbf{r}_2;)/n_1^2, \quad (\text{A9}) \quad g(\mathbf{r}_1 - \mathbf{r}_2, \mathbf{r}_1 - \mathbf{r}_3) = f_3(\mathbf{r}_1, \mathbf{r}_2, \mathbf{r}_3;)/n_1^3, \quad (\text{A12})$$

$$h(\mathbf{r}_1 - \mathbf{r}'_1) = f_2(\mathbf{r}_1; \mathbf{r}'_1)/(n_1 n_2), \quad (\text{A10}) \quad q(\mathbf{r}_1 - \mathbf{r}'_1) = f_3(\mathbf{r}_1, \mathbf{r}_2; \mathbf{r}'_1)/(n_1^2 n_2), \quad (\text{A13})$$

$$f(\mathbf{r}'_1 - \mathbf{r}'_2) = f_2(; \mathbf{r}'_1, \mathbf{r}'_2)/n_2^2, \quad (\text{A11}) \quad p(\mathbf{r}_1 - \mathbf{r}'_1, \mathbf{r}_1 - \mathbf{r}'_2) = f_3(\mathbf{r}_1; \mathbf{r}'_1, \mathbf{r}'_2)/(n_1 n_2^2). \quad (\text{A14})$$

REFERENCES

- Agranovich, V. M., and M. D. Galanin. 1982. Electron Excitation Energy Transfer in Condensed Matter. North-Holland, Amsterdam, 371 pp.
- Agranovich, V. M., and N. A. Efremov. 1980. Luminescence spectra of noncoherent Frenkel excitons at high pumping levels. *Soviet Physics-Solid State*. 22:583–588.
- Bakker, J. G. C., R. van Grondelle, and W. T. F. den Hollander. 1983. Trapping, loss and annihilation of excitations in photosynthetic systems. II. Experiments with the purple bacteria *Rhodospirillum rubrum* and *Rhodospseudomonas capsulata*. *Biochim. Biophys. Acta*. 725:508–518.
- Becker, M., V. Nagarajan, and W. W. Parson. 1991. Properties of excited-singlet states of bacteriochlorophyll *a* and bacteriopheophytin *a* in polar solvents. *J. Am. Chem. Soc.* 113:6840–6848.
- Borisov, A. Yu., R. A. Gdonas, R. Danielius, A. Piskarskas, A. P. Razjivin, and R. Rotomskis. 1984. Investigation of kinetics of the excited state deactivation in the light-harvesting antenna of chromatophores *Rhodospirillum rubrum* by means of the picosecond differential absorption spectroscopy. *Biofizika* (in Russian). 29:396–402.
- Borisov, A. Yu., R. A. Gdonas, R. V. Danielius, A. S. Piskarskas, and A. P. Razjivin. 1982. Minor component B-905 of light-harvesting antenna in *Rhodospirillum rubrum* chromatophores and the mechanism of singlet-singlet annihilation as studied by difference selective picosecond spectroscopy. *FEBS Lett.* 138:25–28.
- Breton, J., N. E. Geacintov, and C. E. Swenberg. 1979. Quenching of fluorescence by triplet states in chloroplasts. *Biochim. Biophys. Acta*. 548:616–635.
- Davydov, A. S. 1971. Theory of Molecular Excitons. Plenum Press, New York.
- Deinum, G., T. J. Aartsma, R. van Grondelle, and J. Amesz. 1989. Singlet-singlet excitation annihilation measurements on the antenna of *Rhodospirillum rubrum* between 300 and 4 K. *Biochim. Biophys. Acta*. 976:63–69.
- Deinum, G. 1991. Excitation migration in photosynthetic antenna systems. Ph.D thesis. University of Leiden, Leiden, The Netherlands.
- Den Hollander, W. T. F., J. G. C. Bakker, and R. van Grondelle. 1983. Trapping, loss and annihilation of excitations in a photosynthetic system. I. Theoretical aspects. *Biochim. Biophys. Acta*. 725:492–507.
- Dobek, A., J. Deprez, N. E. Geacintov, G. Paillotin, and J. Breton. 1985. Chlorophyll fluorescence in chloroplasts on subnanosecond time-scales probed by picosecond pulse pairs. *Biochim. Biophys. Acta*. 806:81–92.

- Freiberg, A., V. I. Godik, T. Pullerits, and K. Timpmann. 1989. Picosecond dynamics of directed excitation transfer in spectrally heterogeneous light-harvesting antenna of purple bacteria. *Biochim. Biophys. Acta.* 973:93–104.
- Gaididei, Y. B., I. V. Zozulenko, and A. I. Onipko. 1985. Diffusion mediated annihilation reactions via short- and long-range interactions: determination of the correct boundary condition. *Chem. Phys. Lett.* 118:421–426.
- Geacintov, N. E., G. Paillotin, J. Deprez, A. Dobek, and J. Breton. 1984. Picosecond pulse energy dependence of singlet-singlet annihilation and fluorescence in chloroplasts. In *Advances in Photosynthesis Research*. Vol. 1. C. Sybesma, editor. Martinus Nijhoff/Dr. W. Junk Publ. The Hague, The Netherlands. 37–40.
- Godik, V. I., K. Timpmann, and A. Freiberg. 1988. Spectral inhomogeneity of the bacteriochlorophyll absorption band in *Rhodospirillum rubrum* obtained by fluorescence picosecond spectroscopy data. *DokLAN SSSR.* 298:1469–2473.
- Gulbinas, V., L. Valkunas, and R. Gadonas. 1994. Local heating and nonlinear annihilation in molecular aggregates. *Lith. J. Phys.* 34: 348–360.
- Hemenger, R. P., R. M. Pearlstein, and K. Lakatos-Lindenberg. 1972. Incoherent exciton quenching on lattices. *J. Math. Phys.* 13:1056–1063.
- Holzwarth, A. R. 1991. Excited-state kinetics in chlorophyll systems and its relationship to the functional organization of the photosystems. In *Chlorophylls*. H. Scheer, editor. CRC Press, Boca Raton, FL. 1125–1151.
- Katoh, R., and M. Kotani. 1993. Observation of fluorescence from higher excited states in an anthracene crystal. *Chem. Phys. Lett.* 201:141–144.
- Kudzmanuskas, S., V. Liuolia, G. Trinkunas, and L. Valkunas. 1985. Nonlinear phenomena in chromatophores of photosynthetic bacteria excited by picosecond laser pulses. *Phys. Lett.* 111A:378–381.
- Kudzmanuskas, S., V. Liuolia, G. Trinkunas, and L. Valkunas. 1986. Minor component of the difference absorption spectra of photosynthetic bacteria chromatophores and nonlinear effect during excitation. *FEBS Lett.* 194:205–209.
- Kudzmanuskas, S., V. Liuolia, G. Trinkunas, and L. Valkunas. 1988. Nonlinear phenomena in picosecond spectroscopy of photosynthetic membranes. In *Proceedings of the Five Ultrafast Phenomena in Spectroscopy (UPS) Topical Meeting*. Z. Rudzikas, A. Piskarskas, and R. Baltramiejunas, editors. World Scientific Co., Singapore. 248–256.
- Mauzerall, D. 1976. Fluorescence and multiple excitation in photosynthetic systems. *J. Phys. Chem.* 80:2306–2309.
- Mauzerall, D. 1982. Statistical theory of the effects of multiple excitation in photosynthetic systems. In *Biological Events Probed by Ultrafast Laser Spectroscopy*. R. R. Alfano, editor. Academic Press, New York. 215–235.
- Mineev, A. P., and A. P. Razjivin. 1987. Statistics of the photon distribution in the set of photosynthetic antenna domains. *FEBS Lett.* 223: 187–190.
- Monger, T. G., and W. W. Parson. 1977. Singlet-triplet fusion in *Rhodospseudomonas sphaeroides* chromatophores. A probe of the organization of the photosynthetic apparatus. *Biochim. Biophys. Acta.* 460:393–407.
- Nuijs, A. M., R. van Grondelle, H. L. P. Joppe, A. C. Bochove, and L. N. M. Duysens. 1985. Singlet and triplet excited carotenoid and bacteriochlorophyll of the photosynthetic purple bacterium *Rhodospirillum rubrum* as studied by picosecond absorbance difference spectroscopy. *Biochim. Biophys. Acta.* 810:94–105.
- Ovchinnikov, A. A., S. F. Timashev, and A. A. Belyi. 1989. Kinetics of diffusion-controlled chemical processes. Nova, New York.
- Paillotin, G., C. E. Swenberg, J. Breton, and N. E. Geacintov. 1979. Analysis of picosecond laser-induced fluorescence phenomena in photosynthetic membranes utilizing a master equation approach. *Biophys. J.* 25:513–534.
- Paillotin, G., N. E. Geacintov, and J. Breton. 1983. A master equation theory of fluorescence induction, photochemical yield, and singlet-triplet exciton quenching in photosynthetic systems. *Biophys. J.* 44:65–77.
- Pullerits, T., and A. Freiberg. 1991. Picosecond fluorescence of simple photosynthetic membranes: evidence of spectral inhomogeneity and directed energy transfer. *Chem. Phys.* 149:409–418.
- Pullerits, T., and A. Freiberg. 1992. Kinetic model of primary energy transfer and trapping in photosynthetic membranes. *Biophys. J.* 63: 879–896.
- Somsen, O. J. G., F. van Mourik, R. van Grondelle, and L. Valkunas. Energy migration, and trapping in a spectrally, and spatially inhomogeneous light-harvesting antenna. *Biophys. J.* 66:1580–1596.
- Suna, A. 1970. Kinematics of exciton-exciton annihilation in molecular crystals. *Phys. Rev. B.* 1:1716–1739.
- Timpmann, K., A. Freiberg, and V. I. Godik. 1991. Picosecond kinetics of light excitations in photosynthetic purple bacteria in the temperature range of 300–4 K. *Chem. Phys. Lett.* 182:617–622.
- Trinkunas, G., and L. Valkunas. 1989. Exciton-exciton annihilation in picosecond spectroscopy of molecular systems. *Exp. Tech. Phys.* 37: 455–458.
- Valkunas, L., S. Kudzmanuskas, and V. Liuolia. 1986. Noncoherent migration of exciton in impure molecular structures. *Liet. Fiz. Rink. (Sov. Phys.-Coll.)* 26:1–11.
- Valkunas, L. 1989. Nonlinear processes in picosecond spectroscopy of photosynthetic systems. In *Proceedings of the 5th International School on Quantum Electronics*. A. Y. Spaser, editor. World Scientific Co, Singapore. 541–560.
- Valkunas, L., V. Liuolia, and A. Freiberg. 1991. Picosecond processes in chromatophores at various excitation intensities. *Photosynth. Res.* 27: 83–95.
- Valkunas, L., F. van Mourik, and R. van Grondelle. 1992. On the role of spectral and spatial antenna in the process of excitation energy trapping in photosynthesis. *J. Photochem. Photobiol. B. Biol. Sci.* 15:159–170.
- Van Grondelle, R. 1985. Excitation energy transfer, trapping and annihilation in photosynthetic systems. *Biochim. Biophys. Acta.* 811:147–195.
- Van Grondelle, R., H. Bergström, V. Sundström, and T. Gillbro. 1987. Energy transfer within the bacteriochlorophyll antenna of purple bacteria at 77 K, studied by picosecond absorption recovery. *Biochim. Biophys. Acta.* 894:313–326.
- Van Grondelle, R., and V. Sundström. 1991. In *Chlorophylls*. H. Scheer, editor. CRC Press, Boca Raton, FL.
- Van Grondelle, R., J. P. Dekker, T. Gillbro, and V. Sundström. 1994. Energy transfer and trapping in photosynthesis. *Biochim. Biophys. Acta.* 1187:1–65.
- Van Mourik, F., R. W. Visschers, and R. van Grondelle. 1992. Energy transfer and aggregate size in the inhomogeneously broadened core light-harvesting complex of *Rhodobacter sphaeroides*. *Chem. Phys. Lett.* 195:1–7.
- Visscher, K. J., H. Bergström, V. Sundström, C. N. Hunter, and R. van Grondelle. 1989. Temperature dependence of energy transfer from the long wavelength antenna Bchl-896 to the reaction center in *Rhodospirillum rubrum*, *Rhodobacter sphaeroides* (w.t. and M21 mutant) from 77K to 177K, studied by picosecond absorption spectroscopy. *Photosynth. Res.* 22:211–217.
- Visschers, R. W., M. C. Chang, F. van Mourik, P. S. Parkes-Loach, B. A. Heller, P. A. Loach, and R. van Grondelle. 1991. Fluorescence polarization and low-temperature absorption spectroscopy of a subunit form of light-harvesting complex I from purple bacteria. *Biochemistry.* 30: 5736–5742.
- Werst, M., Y. W. Jia, L. Mets, and G. R. Fleming. 1992. Energy transfer and trapping in the photosystem I core antenna. A temperature study. *Biophys. J.* 61:868–878.